Distributed Current Estimates Using Cortical Orientation Constraints

Fa-Hsuan Lin,* John W. Belliveau, Anders M. Dale, and Matti S. Hämäläinen

MGH/MIT/HMS Athinoula A. Martinos Center for Biomedical Imaging, Charlestown, Massachusetts

Abstract: Distributed source models of magnetoencephalographic (MEG) and electroencephalographic (EEG) data employ dense distributions of current sources in a volume or on a surface. Previously, anatomical magnetic resonance imaging (MRI) data have been used to constrain locations and orientations based on cortical geometry extracted from anatomical MRI data. We extended this approach by first calculating cortical patch statistics (CPS), which for each patch corresponding to a current source location on the cortex comprise the area of the patch, the average normal direction, and the average deviation of the surface normal from its average. The patch areas were then incorporated in the forward model to yield estimates of the surface current density instead of dipole amplitudes at the current locations. The surface normal data were employed in a loose orientation constraint (LOC), which allows some variation of the current direction from the average normal. We employed this approach both in the ℓ^2 minimum-norm estimates (MNE) and in the more focal ℓ^1 minimum-norm solutions, the minimum-current estimate (MCE). Simulations in auditory and somatosensory areas with current dipoles and 10- or 20-mm diameter cortical patches as test sources showed that applying the LOC can increase localization accuracy. We also applied the method to in vivo auditory and somatosensory data. *Hum Brain Mapp 27:1–13, 2006.*

Key words: inverse; MEG; cortical constraints; MNE; MCE; minimum norm; brain

INTRODUCTION

Magnetoencephalography (MEG) is a noninvasive tool to investigate the human brain function with millisecond temporal resolution [Cohen, 1968; Hämäläinen et al., 1993] by measuring magnetic fields ensuing from the neural currents in the brain. MEG is closely related to electroencephalography (EEG), which measures the electric potential distributions generated by the same sources. MEG is selectively sensitive to the source currents that are tangential with respect to the surface of the head, whereas EEG detects both the tangential and radial source components. Localization of the sources with these methods is difficult due to the nonuniqueness of the electromagnetic inverse problem. To render the solution unique, several source models with different constraints have been proposed.

The most popular MEG and EEG source modeling approach is to assume that the extent of activation is small and consequently that the measured fields can be accounted for by modeling the source by a set of equivalent current dipoles (ECDs). If multiple sources are simultaneously active, reliable estimation of the source parameters is difficult because of the nonlinear relationship between the source loca-

Contract grant sponsor: National Institutes of Health; Contract grant number: R01 HD040712, R01 NS037462, P41 RR14075, 1R21EB004965-01; Contract grant sponsor: Mental Illness and Neuroscience Discovery Institute (MIND).

*Correspondence to: Fa-Hsuan Lin, MGH/MIT/HMS Athinoula A. Martinos Center for Biomedical Imaging, Building 149, 13th St. Charlestown, MA 02129. E-mail: fhlin@nmr.mgh.harvard.edu

Received for publication 10 December 2004; Accepted 10 February 2005

DOI: 10.1002/hbm.20155

Published online 4 August 2005 in Wiley InterScience (www.interscience.wiley.com).

tions and the measured signals. Although global optimization algorithms have been tailored to accomplish this task [Uutela et al., 1998], the most feasible solutions combine optimization algorithms with partly heuristic interactive approaches, motivated by prior physiological and anatomical information. In addition, the dipole may be an oversimplification as a model for spatially extended source activity.

To overcome these difficulties, several distributed current solutions have been proposed. A widely employed distributed source localization approach in MEG and EEG is based on the ℓ^2-norm prior, resulting in diffuse minimum-norm estimates (MNE) [Dale and Sereno, 1993; Dale et al., 2000; Hämäläinen and Ilmoniemi, 1984]. More focal estimates can be obtained by using an ℓ^1-norm prior; the corresponding minimum-norm solution is often called the minimum-current estimate (MCE) [Matsuura and Okabe, 1995; Uutela et al., 1999].

It has been proposed previously that individual anatomical information acquired with structural magnetic resonance imaging (MRI) can be incorporated into the source localization with the ℓ^2-norm constraint. In particular, the locations of the sources can be constrained to the cortical mantle and their orientations to be perpendicular to the local cortical surface [Dale and Sereno, 1993]. Such a modeling constraint is motivated by the physiological information that the most significant sources of MEG and EEG signals are postsynaptic currents in the pyramidal cells on the cortex and that the principal net direction of these currents is perpendicular to the cortical surface [Hämäläinen et al., 1993; Okada et al., 1997]. Importantly, in MCE, the optimization algorithm becomes more straightforward if the orientations of the sources are known and the source amplitudes subsequently estimated subject to the ℓ^1 constraint. To this end, the MCE implementation described in Uutela et al. [1999] used the current-source orientations provided by MNE.

To maintain computational efficiency, distributed source models usually employ a spacing of 5–10 mm between neighboring sources in the discrete source space. In our previous work with the minimum ℓ^2-norm estimate [Dale et al., 2000], we employed the cortical location constraint with current orientations either unconstrained or strictly constrained to the orientation of the cortical normal at each source space point. Using a strict orientation constraint is sensitive to the sampling algorithm used in the creation of source space, because it does not take into account the fact that the orientation may vary considerably within each typically 5–10-mm diameter cortical patch corresponding to each of the source space points. In addition, misalignment of the MEG/EEG and MRI coordinate frames is more critical when the orientations are strictly constrained because the magnetic field and electric potential patterns are very sensitive to the orientations of the currents [Hämäläinen et al., 1993].

To overcome the problems associated with the strict cortical orientation constraint, we calculate *cortical patch statistics* (CPS), which quantifies the variation of the surface normal within each cortical patch. We incorporate the refined normal information in the minimum-norm inverse solutions as the *loose orientation constraint* (LOC). We employ this new approach in the calculation of both ℓ^1- and ℓ^2-norm distributed solutions. In the sequel, we present the technical details of our approach, followed by simulations on both auditory and somatosensory cortex with different source configurations. Finally, analysis of auditory and somatosensory MEG data will be presented to demonstrate the utility of the approach.

DISTRIBUTED INVERSE SOLUTIONS

Minimum-Norm Estimates

The measured MEG/EEG signals and the underlying current source strengths are related by the linear transformation:

$$\mathbf{Y} = \mathbf{AX} + \mathbf{N}, \tag{1}$$

where $\mathbf{Y}$ is an m-by-t matrix containing measurements from m sensors over t distinct time instants, $\mathbf{X}$ is a $3n$-by-t matrix denoting the unknown time-dependent amplitudes of the three components of n current sources, $\mathbf{A}$ is the gain matrix representing the mapping from the currents to MEG/EEG signals, i.e., the solution of the forward problem, and $\mathbf{N}$ denotes noise in the measured data. The most feasible assumption is that $\mathbf{N}$ is Gaussian with a spatial covariance matrix $\mathbf{C}$, to be estimated from the data. If we further assume that the source amplitudes have a Gaussian a priori distribution with a covariance matrix $\mathbf{R}$, we obtain the Bayesian maximum a posteriori (MAP) estimate or ℓ^2 minimum-norm solution, linearly related to the measurements, as [Dale and Sereno, 1993]

$$\mathbf{X}^{\mathrm{MNE}} = \mathbf{RA}^T(\mathbf{ARA}^T + \lambda^2\mathbf{C})^{-1}\mathbf{Y} = \mathbf{WY}, \tag{2}$$

where λ^2 is a regularization parameter to avoid magnification of errors in data in the current solution and the superscript T indicates the matrix transpose. We have also implicitly assumed that $\mathbf{C}$ and $\mathbf{R}$ are time independent and that there are no temporal correlations. In the original unweighted minimum-norm approach, $\mathbf{R}$ is simply a multiple of the identity matrix; however, there is no direct physiological information to support this selection of the source priors. Rather, the choice is motivated by the simple computational realization of the estimation procedure. Consequently, we prefer not to emphasize here the Bayesian interpretation of the MNE.

Equation (2) can be also viewed as the analytic solution of an optimization problem where the cost function is a sum of weighted least-squares error between the measured and modeled data and a penalty term consisting of the power of the estimated currents. In the subsequent section of MCE, we will consider another source prior, namely the ℓ^1-norm prior, which corresponds to a double-exponential probabil-

ity distribution function with zero mean as discussed in Uutela et al. [1999]. In MCE, the penalty term is the sum of the absolute values of the source currents whereas the data error term is identical to that in MNE. The two approaches can thus be regarded as two variants of distributed source modeling techniques with distinct prior assumptions.

In the calculation of the gain matrix **A**, a common practice is to assume dipolar sources in a dense grid covering either the entire brain or the cortical mantle. In this approach, the current estimates are dipole amplitudes, whose unit is [Am]; however, a more appropriate quantity to consider is the volume or surface dipole density given in [Am/m^3] or [Am/m^2], respectively. In case of cortically constrained currents, transformation to current density representation requires an approximation for the area of the cortical patch corresponding to each source location. We compute these patch areas using detailed cortical geometry information, as will be described below. The transformation is accomplished by multiplying each column of a "dipolar" gain matrix by the corresponding patch area. In the following discussion, we assume that the current density transformation has been already included in **A**. This transformation does not involve changes to **R**, because in the original formulation the assumption of equal variances across the source space was actually not justified due to the potentially varying patch sizes. In our implementation, we calculated **A** using a single-layer boundary element model (BEM) assuming the shape of the inner skull surface [Hämäläinen and Sarvas, 1989; Oostendorp and van Oosterom, 1989].

In Equation (2), the current orientations have not been constrained. A priori orientation information can be easily incorporated by replacing the gain matrix by

$$\mathbf{A}_{\text{fixed}} = \mathbf{A}\Theta\,, \tag{3}$$

where Θ is the $3n$-by-n matrix containing the unit vectors pointing to the directions of the currents. If the direction cosines of the kth dipole are c_{kx}, c_{ky}, and c_{kz}, the kth column of Θ reads

$$\Theta_k = (\underbrace{0\ldots0}_{3(k-1)}\ c_{kx}\quad c_{ky}\quad c_{kz}\quad \underbrace{0\ldots0}_{n-3k})^{\mathrm{T}}\,. \tag{4}$$

Instead of applying Equation (2) directly, it is convenient to use an equivalent formulation

$$\mathbf{X}^{\mathrm{MNE}} = \mathbf{R}\tilde{\mathbf{A}}^T(\tilde{\mathbf{A}}\mathbf{R}\tilde{\mathbf{A}}^T + \lambda^2\mathbf{I})^{-1}\tilde{\mathbf{Y}} = \tilde{\mathbf{W}}\tilde{\mathbf{Y}}\,, \tag{5}$$

where

$$\begin{aligned}\tilde{\mathbf{Y}} &= \mathbf{C}^{-1/2}\mathbf{Y}\\ \tilde{\mathbf{A}} &= \mathbf{C}^{-1/2}\mathbf{A}\end{aligned} \tag{6}$$

are the spatially whitened data and spatially whitened gain matrix, respectively. The noise-covariance matrix of the whitened data is an identity matrix, as indicated by the comparison of Equations (2) and (5). The whitening procedure also allows one to use the scaling $\lambda^2 = \zeta^2\mathrm{tr}(\tilde{\mathbf{A}}\mathbf{R}\tilde{\mathbf{A}}^T)/\mathrm{m}$, where ζ^2 denotes the inverse of the signal-to-noise ratio (SNR) of the whitened data, to bring the regularization parameter to a reasonable scale even in cases where the measurements have different units of measure, which is the case when planar gradiometer and magnetometer data or MEG and EEG data are combined in a single estimate.

The MNE is known to have a bias toward superficial currents caused by the attenuation of the MEG and EEG lead fields with increasing source depth. It is possible to compensate for this tendency by modifying our diagonal source-covariance matrix **R** by scaling the entries by a function increasing monotonically with source depth, denoted here by f_k for the kth source. A commonly used choice is

$$f_k = \Delta_k^{2\gamma}/(\boldsymbol{a}_{3k-2}^T\boldsymbol{a}_{3k-2} + \boldsymbol{a}_{3k-1}^T\boldsymbol{a}_{3k-1} + \boldsymbol{a}_{3k}^T\boldsymbol{a}_{3k})^{\gamma}\,, \tag{7}$$

where $\boldsymbol{a}_p$ is the pth column of **A** (the gain matrix with patch sizes taken into account), Δ_k is the corresponding cortical patch size, and γ is a tunable parameter. The depth weighting in Equation (7) is independent of the patch size. Although Fuchs et al. [1999] suggest that $\gamma = 1$, we have found in our simulations that this does not provide sufficient compensation. Our preferred value is slightly bigger ($\gamma \sim 1.4$) [Lin et al., 2004]. In Equation (7), we have effectively employed the dipolar gain matrix because two sources at the same depth should receive the same weight independent of the source patch size.

Noise-Normalized MNE

In the above, Equations (2) and (5) provide the best-fitting values of the amplitudes or, in Bayesian view, the maximum a posteriori (MAP) estimate. To make the resulting maps conceptually similar with those calculated in other functional imaging modalities, Dale et al. [2000] proposed that current values should be converted into dynamic statistical parametric maps. To this end, we need to consider the variances of the currents

$$w_k = (\mathbf{W}\mathbf{C}\mathbf{W}^T)_{kk} = (\tilde{\mathbf{W}}\tilde{\mathbf{W}}^T)_{kk}\,. \tag{8}$$

For fixed-orientation sources, we now obtain the noise-normalized activity estimate for the kth dipole and pth time point as

$$z_{kp} = \frac{X_{k,p}^{\mathrm{MNE}}}{w_k}\,, \tag{9}$$

which is t distributed under the null hypothesis of no activity at the location k. Because the number of time samples used to calculate the noise-covariance matrix **C** is quite large

(more than 100), the t distribution approaches a unit normal distribution (i.e., a z score).

If the orientation is not constrained, the noise-normalized solution is calculated as

$$F_{kp} = \frac{\sum_{q=1}^{3} (X^{\mathrm{MNE}}_{3(k-1)+q,p})^2}{\sum_{q=1}^{3} w^2_{3(k-1)+q}}. \quad (10)$$

Under the null hypothesis, F_{kp} is F distributed, with three degrees of freedom for the numerator. The degree of freedom for the denominator is typically large, again depending on the number of time samples used to calculate the noise-covariance matrix.

As discussed in Dale et al. [2000], the noise-normalized estimates resulting from the transformations given in Equations (9) and (10) have a smaller depth bias than do the MNEs obtained without applying depth weighting. Furthermore, the point-spread function, i.e., the image of a point current source, is more uniform in space in the noise-normalized estimate than it is in the MNE.

Minimum-Current Estimates

In contrast to the MNE, the MCE employs the ℓ^1-norm as constraint [Matsuura and Okabe, 1995; Uutela et al., 1999]. Mathematically, MCE can be formulated as the solution of the optimization problem:

$$\mathbf{X}^{\mathrm{MCE}}_p = \underset{x_{i,p}}{\operatorname{argmin}} \left\{ \sum_{i=1}^{n} w_i |X_{i,p}| \right\}, \quad (11)$$

$$\text{subject to } \tilde{\mathbf{Y}}_{rp} = \mathbf{B}_r \mathbf{X}^{\mathrm{MCE}}_p$$

where $\mathbf{X}^{\mathrm{MCE}}_p$ is the solution at time point p and w_i are the weights of dipole sources, whereas $\tilde{\mathbf{Y}}_{rp}$ and $\mathbf{B}_r$ are derived from the measurement data and the forward solution for fixed-orientation sources to implement regularization as follows. As before, let Θ be the n-by-3 matrix containing the source orientations and compute the singular-value decomposition

$$\tilde{\mathbf{A}}\Theta = \mathbf{U}\Pi\mathbf{V}^T. \quad (12)$$

Then

$$\mathbf{B}_r = \mathbf{U}_r^T \tilde{\mathbf{A}}\Theta$$
$$\tilde{\mathbf{Y}}_r = \mathbf{U}_r^T \tilde{\mathbf{Y}}, \quad (13)$$

where $\mathbf{U}_r$ is composed of the first r columns of $\mathbf{U}$. This method of eigenvalue truncation in regularization was introduced to MCE by Uutela et al. [1999], and it is closely related to using the regularization parameter λ^2 in Equations (2) and (5). It is easy to show that the latter corresponds to weighting of the eigenvalues with a smooth transition function instead of the step function implied by Equation (13).

We selected λ^2 and the truncation point for the MCE regularization so that in both cases, 99% of the total lead field power was included in the estimation. Specifically, λ^2 was first decided from the whitened data in MNE. For the smooth regularization function employed in MNE, the relationship between λ^2 and the amount of lead field power included is

$$p_{\mathrm{MNE}} = \frac{\sum_{k=1}^{m} \frac{\lambda_k^2}{\lambda_k^2 + \lambda^2} \lambda_k^2}{\sum_{k=1}^{m} \lambda_k^2}, \quad (14)$$

where λ_k are the singular values of $\tilde{\mathbf{A}}\mathbf{R}^{\frac{1}{2}}$. For the truncation in MCE, we select r such that

$$p_{\mathrm{MNE}} \approx p_{\mathrm{MCE}}$$

$$p_{\mathrm{MCE}} = \frac{\sum_{k=1}^{r} \pi_k^2}{\sum_{k=1}^{m} \pi_k^2}, \quad (15)$$

where π_k are the singular values of $\tilde{\mathrm{A}}\Theta$, i.e., the diagonal elements of Π defined in Equation (12).

The above implementation of MCE requires the knowledge of the source orientations, to be incorporated by the matrix Θ in Equations (12) and (13). In principle, it is also possible to implement MCE without requiring Θ to be specified first. The solution of this minimization problem is numerically demanding; therefore, we prefer using the original MCE formulation proposed by Uutela et al. [1999].

The weights for currents, w_i in Equation (11), were the Euclidean norms of the columns of $\mathbf{A}\Theta$. The orientation matrix Θ was obtained either from an initial MNE using free orientation, loose cortical orientation constraint, or strict cortical orientation constraint (see section below). In line with Uutela et al. [1999], we employed linear programming [Moon and Stirling, 2000] to estimate the magnitudes of dipole sources.

REFINED CORTICAL CONSTRAINTS

Representation of the Cortical Surfaces

As described in the previous section, a feasible anatomical constraint for MEG and EEG source localization is to restrict

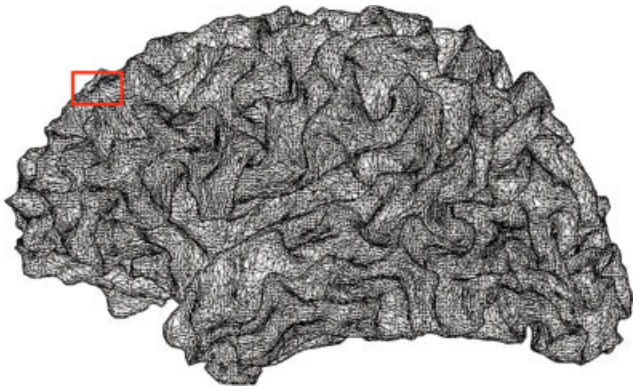

Figure 1.
The triangulated left-hemisphere white-matter surface derived from high-resolution T1-weighted MRI. The red box indicates the region to introduce the definition of local cortical patch (see Fig. 2). [Color figure can be viewed in the online issue, which is available at www.interscience.wiley.com.]

the source locations to the cortical mantle, extracted from the individual's MRI. With modern segmentation methods, a representation for the geometry of the cortex can be automatically generated from high-resolution 3-D MRI data sets. We employed the FreeSurfer software [Dale et al., 1999; Fischl et al., 1999, 2001] to build the triangular cortical surface mesh from T1-weighted anatomical 3-D volume MRI data (magnetization prepared rapid acquisition gradient echo [MPRAGE] sequence, repetition time/echo time [TR/TE] = 2,530/3.49 ms, flip angle = 7 degrees, partition thickness = 1.33 mm, matrix = 256 × 256, 128 partitions, and field of view = 21 cm × 21 cm) acquired in a 1.5-T MRI scanner (SIEMENS Medical Solutions, Erlangen, Germany) with a 1-mm isotropic spatial resolution. The principal surfaces generated by FreeSurfer are the pial surface and the gray–white matter boundary; we used the latter to generate the cortically constrained source space. We confirmed the accuracy of the segmentation by superimposing the locations of the vertices of the triangulation on the original MRI slices and found that the quality of the segmentation was excellent, as also discussed in Dale et al. [1999].

In addition to the folded surface, FreeSurfer also computes inflated and flattened representations of the cortex, which expose the parts of the cortex embedded in the sulci. These representations are thus particularly useful for visualizing MEG data, which are sensitive mainly to fissural activity.

To achieve sufficient anatomical detail, the triangular tessellations of the cortical surfaces consisted of around 130,000–150,000 vertices per hemisphere, corresponding to an approximate triangle size of 1 mm. For source modeling,

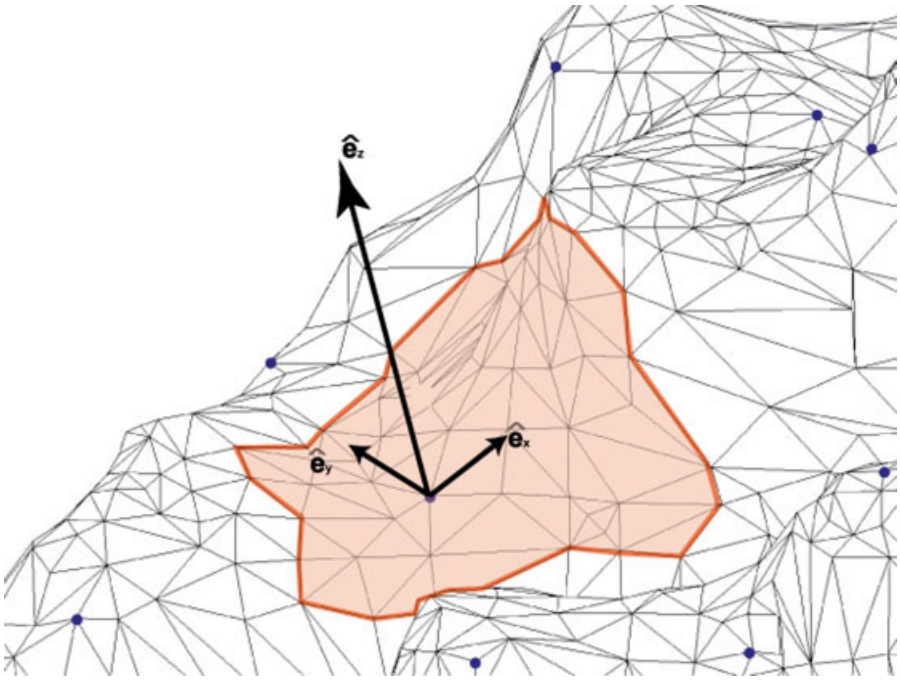

Figure 2.
A cortical patch bounded by the thick red lines. Blue spots denote the locations of the sources after 10-mm decimation. A Cartesian coordinate system with z-direction aligned with the average normal direction is indicated with the black arrows. [Color figure can be viewed in the online issue, which is available at www.interscience.wiley.com.]

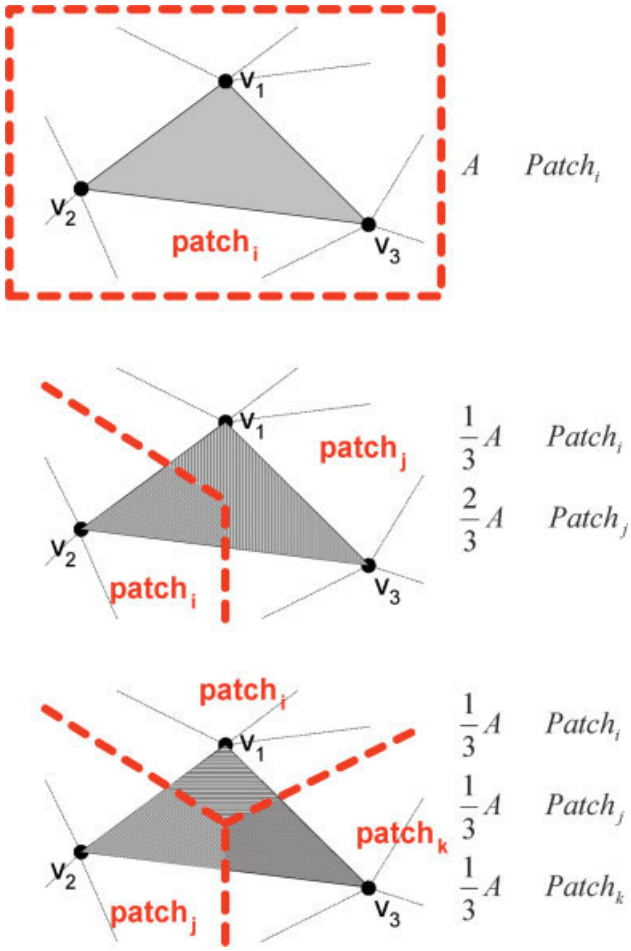

Figure 3.
The division of a cortical surface triangle with area A and vertices V_1, V_2, and V_3 to different cortical patches. The red dashed lines indicate the boundaries between cortical patches. [Color figure can be viewed in the online issue, which is available at www.interscience.wiley.com.]

this dense triangulation was subsequently decimated to a source space of approximately 7,500 dipoles with 7-mm distance between the nearest two dipoles. The decimation was motivated by the limited spatial resolution intrinsic to the source localization using MEG/EEG and practical computational efficiency concerns. However, this simplified source geometry may yield inaccurate dipole orientations that do not take into account the orientation variation over the patch belonging to each decimated current source location. Furthermore, the actual areas of the patches have to be taken into account in the calculations to correctly estimate the current density on the cortex.

Cortical Patch Statistics

To acquire more representative cortical information, we used the original dense cortical mesh to obtain a characterization of the cortical patches. We employed the Dijsktra algorithm [Bertsekas, 2000] along the edges of the cortical mesh to calculate the distance from all vertices to each of the decimated source points. For each vertex of the original cortical mesh, the closest decimated dipole location was thus determined. A cortical patch P_d can be now defined by the set of vertices in the original dense triangulation sharing the same nearest decimated dipole location, as shown in Figures 1 and 2. We computed four quantities for each cortical patch associated with the decimated source locations: the number of vertices in each patch, N_d; the patch size, Δ_d; the average vertex normal, $\bar{\mathbf{n}}_d$; and the average deviation of the vertex normals from their average, σ_d. We refer to these data collectively as the CPS.

Given the cortical patch definitions across the whole cortical mantle, Δ_d are calculated by including the area of each surface triangle to the area of the patch to which it belongs. At the boundary of the cortical patch, the area of the triangle was divided proportional to the number of vertices belonging to the same cortical patch, as shown in Figure 3. The remaining quantities included in CPS are defined as

$$\bar{\mathbf{n}}_d = \frac{1}{N_d}\sum_{k\in P_d}\hat{\mathbf{n}}_k \Big/ \left\|\frac{1}{N_d}\sum_{k\in P_d}\hat{\mathbf{n}}_k\right\|, \qquad (16)$$

$$\sigma_d = \frac{1}{N_d}\sum_{k\in P_d}\arccos(\hat{\mathbf{n}}_k\cdot\bar{\mathbf{n}}_d)$$

where $k\in p_d$ defines the vertices in patch d, $\hat{\mathbf{n}}_k$ is the approximated unit normal vector at vertex k, and $\|\cdot\|$ indicates the length of the enclosed vector.

Figure 4 shows the spatial distribution of the cortical patch sizes on an inflated left hemisphere cortical surface.

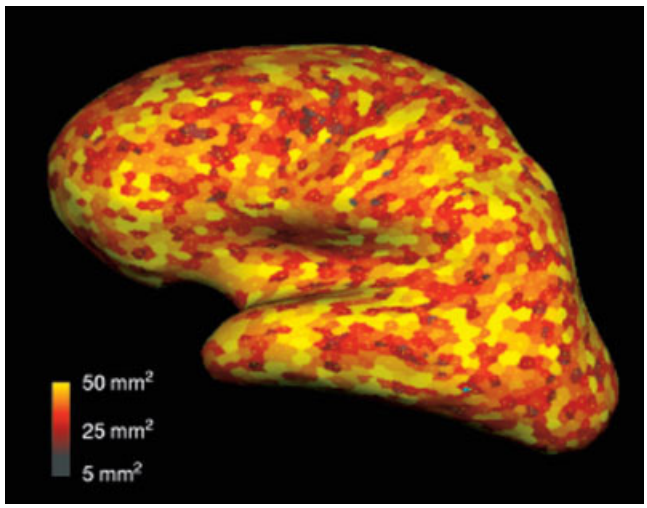

Figure 4.
The spatial distribution of the cortical patch areas on an inflated left-hemisphere cortical surface.

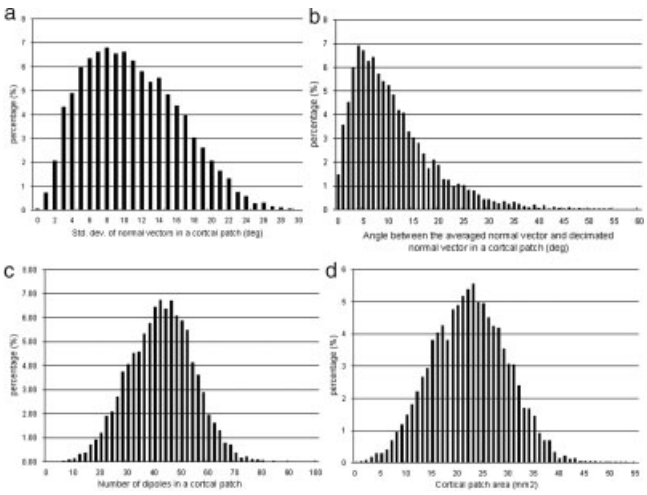

Figure 5.

a: The distribution of the average deviations (σ_d) of the cortical normal from the average normal directions ($\bar{n}_d$). **b:** The distribution of angles between $\bar{n}_d$ and the dipole orientations at the decimated surface points. **c:** The distribution of the number of dipoles in a cortical patch (N_d). **d:** The distribution of the areas of the cortical patches (Δ_d).

This figure indicates that the distribution of the patch areas is not systematic and that adjacent patches can have substantial size differences. Figure 5a shows the distribution of σ_d in one subject. The data were obtained by decimating the original dense triangulation to an approximate source grid spacing of 7 mm. In 99% of the patches, $\sigma_d < 25$ degrees. The median of this distribution is 10 degrees. Figure 5b shows the distribution angles between $\bar{\mathbf{n}}_d$ and the normal vectors at the decimated source locations. Mostly, such a deviate is between 5–10 degrees with a median of 8 degrees. In about 3% of the decimated sources, the averaged normal deviates from the source location normal as much as 30 degrees. Figure 5c shows the distribution N_d. On the average, a cortical patch contains 40 vertices when we employ a 7-mm decimation. Cortical patches with less than 20 and more than 60 vertices constitute only approximately 5% of the total number of patches. The distribution of Δ_d is shown in Figure 5d. With 7-mm decimation, the patches have an averaged area of 22.76 mm^2. The standard deviation of the distribution is 7.4 mm^2.

Computation of the patch statistics needs to be carried out only once per each subject and source decimation. With 7-mm source spacing, the computation takes about 9 min on a 1.4-GHz AMD Athlon processor. The computational penalty in the subsequent calculation of the MNE and MCE solutions is negligible.

Loose Orientation Constraint

Rather than assigning a fixed orientation to decimated dipole directly, we employ the average orientation $\bar{\mathbf{n}}_d$ within a patch to reduce the effect of sampling the original tessellation. To accommodate further the deviation σ_d from the average normal direction in each cortical patch, we use an LOC as follows:

$$\mathbf{R}^{cort}_{\{d,d\}} = [\sin\theta_d \ \sin\theta_d \ 1]$$

$$\tilde{\mathbf{A}}^{cort}_{\{d\}} = \tilde{\mathbf{A}}_{\{d\}}[\hat{e}_{x,d} \ \hat{e}_{y,d} \ \hat{e}_{z,d}] \tag{17}$$

$$\mathbf{X} = \mathbf{R}^{cort}\tilde{\mathbf{A}}^{cort^T}(\tilde{\mathbf{A}}^{8cort}\mathbf{R}^{cort}\tilde{\mathbf{A}}^{cort^T} + \lambda^2\mathbf{I})^{-1}\tilde{\mathbf{Y}}$$

where $\mathbf{R}_{\{d,d\}}$ are the three diagonal elements of $\mathbf{R}$ corresponding to one dipole and d denotes the column indices for one dipole in the forward matrix. $[\hat{e}_{x,d} \ \hat{e}_{y,d} \ \hat{e}_{z,d}]$ is a rotation matrix with $\hat{e}_{z,d} = \bar{\mathbf{n}}_d$, the average cortical normal direction over a cortical patch, $\hat{e}_{x,d}$ and $\hat{e}_{y,d}$ being perpendicular to it in the "tangential" plane. The quantity $\sin\theta_d$ ranges from 0 to 1 as $0 \leq \theta_d \leq 90$ degrees. The reason for using the sine function here is that we will later relate θ_d and σ_d, given as an angle, by constant factor: $\theta_d = \beta\sigma_d$. As a result, we obtain three alternatives for computing the cortically constrained MNE: without an orientation constraint, with fixed orientation constraint taken as samples from the complete cortical triangulation, and the LOC. In the sequel, we refer to the three methods as free orientations (FO), strict orientation constraint (SOC), and LOC, respectively. In terms of Equation (17), $\sin\theta_d = 1$ for FO, $\sin\theta_d = 0$ for SOC, and $0 < \sin\theta_d < 1$ for LOC.

Refined Cortical Constraints and MCE

In the original implementation of MCE, an MNE with unconstrained source orientations was employed to estimate the dipole orientations for the computation of MCE. Linear programming (LP) was used subsequently to solve the minimization problem in Equation (11) [Uutela et al., 1999]. In this approach, no cortical location or orientation constraint was used; the source space consisted of an even 3-D grid of locations covering the brain. In our simulation and real-data examples to follow, we will always constrain the source locations to the cortex. The anatomically informed MCE is computed given the measurement data, the forward solution, and the dipole orientation estimates. The source orientations are obtained by either computing an initial anatomy-informed MNE or by using the cortical normal estimates directly.

We compare three alternatives for the source orientation constraint in the initial MNE, required in the computation of MCE. In the first one, we calculate the MNE without orientation constraint and use the source orientations given by the MNE in the MCE computation. In the second alterative, we use the CPS and the LOC together with the cortical location constraint in the computation of the initial MNE. The incorporation of brain anatomy from the high-resolution MRI with cortical patch definitions is expected to give a better approximation for the dipole orientations than does the unconstrained MNE used in Uutela et al. [1999]. Our third alternative is to use a strict cortical orientation con-

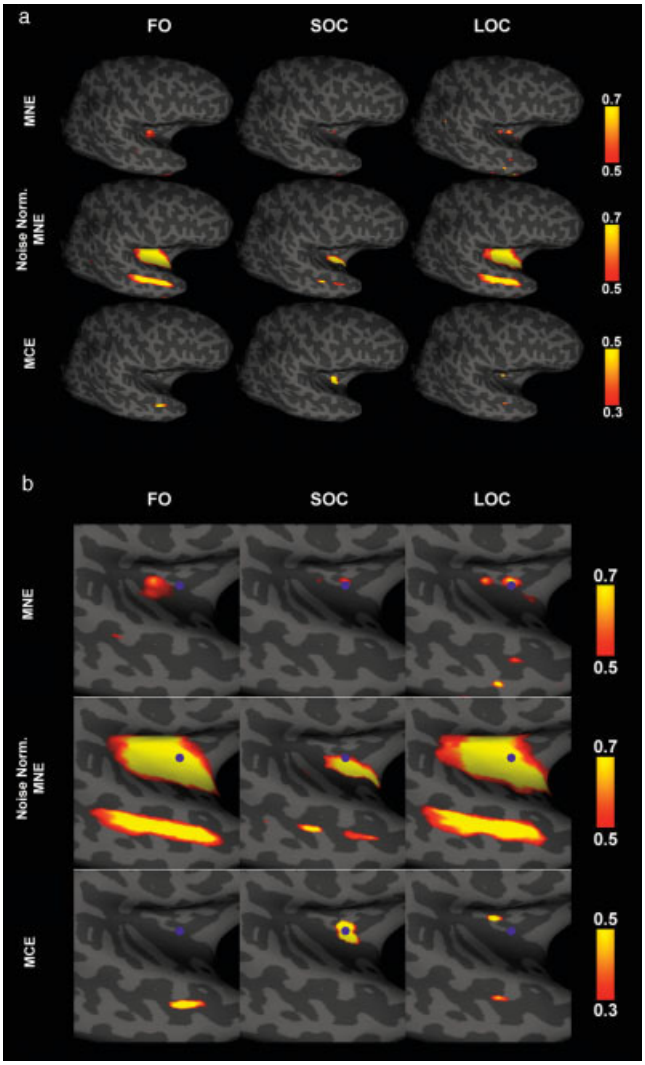

Figure 6.
Comparison of minimum-norm estimates (MNE), noise-normalized MNE, and minimum-current estimate (MCE) computed from simulated data due to a current dipole in the temporal lobe, indicated by a blue dot. Cortical current estimates were normalized between 0 and 1 to illustrate the spatial extent of the distributions.

straint in the MCE calculations directly without computing a MNE first.

Inverse Solution Visualization

To assess the localization precision of using proposed FO, SOC, or LOC in MNE and MCE, we linearly scaled all inverse solutions between 0.0 and 1.0 individually. This assures that the dynamic ranges of the inverse solutions of all variants proposed herein are identical. For illustration, we showed the maximal 50% of the MNE and noise-normalized MNE solutions and the maximal 70% of the MCE solutions. The reason for different threshold values in MNE and MCE is that the MCE solutions are more focal by the nature of ℓ^1 norm prior.

SIMULATIONS

To evaluate the performance of the LOC, we generated simulated MEG data by assuming source in the central sulcus in the regions of the primary somatosensory area (SI) on the left hemisphere and in the Sylvian fissure in the regions of the primary auditory cortex on the right hemisphere. We employed three source configurations: current dipoles, 10-mm diameter patches, and 20-mm diameter patches. The orientations of these simulated sources were adjusted to be perpendicular to the local cortical surface as informed by anatomical MRI. The ideal sensor measurements on MEG sensors were thus calculated using the gain matrix and the source amplitudes. In calculation of the gain matrix, we used the MEG/MRI registration from a realistic 306-channel Vectorview MEG system (Elekta-Neuromag, Ltd., Helsinki, Finland) covering the cerebral cortex evenly. For simulations with patches, we calculated the forward solution in the complete dense cortical grid and placed a

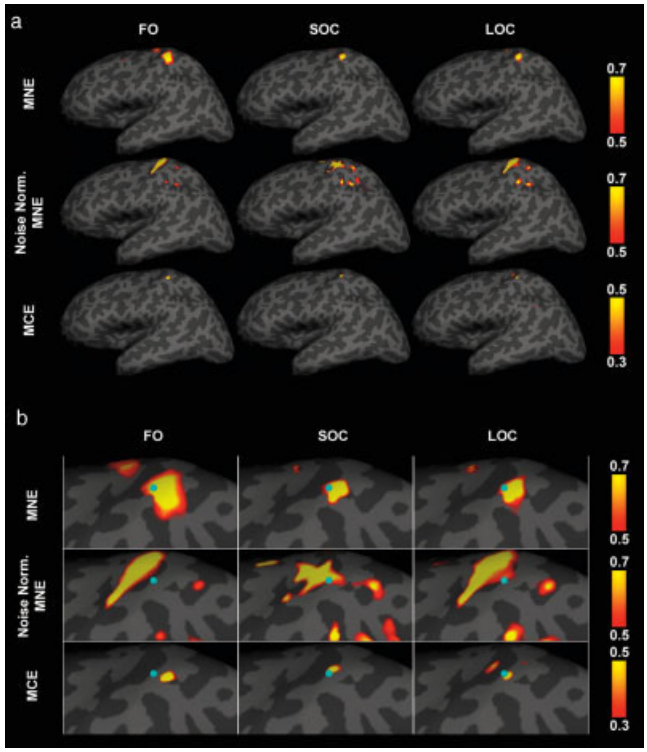

Figure 7.
Comparison of minimum-norm estimates (MNE), noise-normalized MNE, and minimum-current estimate (MCE) computed from simulated data due to a current dipole in the primary somatosensory area (SI) hand area, indicated by a blue dot. Cortical current estimates were normalized between 0 and 1 to illustrate the spatial extent of the distributions.

TABLE I. Shifts of the center of mass (S_{cm}) in millimeters in the auditory cortex and somatosensory cortex simulations

	Auditory cortex			Somatosensory cortex		
Approach	FO	SOC	LOC	FO	SOC	LOC
MNE	17.6	17.2	14.8	10.3	9.6	9.5
Noise-normalized MNE	7.0	6.9	5.6	7.0	4.4	5.3
MCE	16.3	2.6	3.0	6.5	3.0	1.8

FO, free orientation; SOC, strict orientation constraint; LOC, loose orientation constraint; MNE, minimum-norm estimate; MCE, minimum-current estimate.

dipole source of equal amplitude at every vertex within the patch.

To approximate realistic conditions where contaminating noise is present, we superimposed Gaussian noise of zero mean and unit variance on the ideal sensor measurements at power SNR of 100. The definition of SNR here is the ratio between the instantaneous power of the ideal MEG sensor measurements over that of the MEG sensor noises. In our experience, the SNR defined in this way ranges from 4 to 100 in actual MEG studies with 50–200 averages in evoked-response studies. In both auditory and somatosensory data, we typically obtain SNR in the higher end of this range. Our simulations thus correspond well to high-SNR MEG data.

Distributed source estimates were calculated using MNE, noise-normalized MNE [Dale et al., 2000; Liu et al., 2002], and MCE approaches, employing a decimated source space with a 7-mm grid spacing. The orientations of sources were unconstrained, strictly constrained to the average normal within the cortical patch, or loosely constrained using the LOC with $0.5\sigma_d < \theta_d < 5\sigma_d$ in Equation (17). The same multiplier was used for all patches. The precision of localization was evaluated by the distance between the center of mass of the distributed source estimates and the center of mass of the simulated sources. We define this metric as *shift of center of mass* S_{cm} (SCM). To avoid influence from the background insignificant dipole estimates, we used only the dipoles whose amplitudes exceeded 50% of the maximum amplitude. To demonstrate the behavior of the solutions when multiple sources were simultaneously active, we simulated two simultaneously active dipole sources at somatosensory cortex with separation of 21 mm and subsequently localized the synthetic MEG sensor data with free, strict cortical, or loose cortical orientation constraints using MNE, noise-normalized MNE, and MCE.

Figures 6 and 7 show simulation results of MNE, noise-normalized MNE, and MCE using FO, SOC, and LOC for one particular ECD source at auditory cortex or somatosensory cortex, indicated in the Figures by a blue dot. Table I lists the shifts of center of mass using FO, SOC, and LOC for the examples depicted in Figures 6 and 7. In MNE, FO gives the minimal shift of the center of mass. However, when applying noise normalization, FO-MNE yielded the largest S_{cm}. Using LOC, even not giving the minimal S_{cm} in MNE, the shifts remained smaller compared to that for FO inverse solutions. In particular, we emphasize the difference of S_{cm} when applying LOC in contrast to FO or SOC: LOC-MCE results gave minimal S_{cm} in both auditory cortex and somatosensory cortex compared to that with SOC and FO. Traditional MCE using FO-based MNE orientation may generate S_{cm} two- to threefold larger than MCE using LOC-based MNE orientation.

Figure 8 shows and summarizes the simulation results of the locations of 73 simulated sources at SI and 90 simulated sources at auditory cortex. MNE utilizing LOC on single-dipole synthetic data yields the smallest average S_{cm} (11.3 mm in auditory area and 5.8 mm in somatosensory area), compared to MNE using either FO or SOC in both auditory (FO, 11.6 mm; SOC, 12.8 mm) and somatosensory area (FO, 8.5 mm; SOC, 15.2 mm). For LOC we explored the range $0.5\sigma_d < \theta_d < 5\sigma_d$ and found that the median of the optimal θ_d, producing the smallest localization errors, was $\theta_d = 2.0\sigma_\theta$. The effect of decreasing the shift of the center of mass by appropriate LOC was observed systematically with the more extended synthetic sources as well.

Using noise-normalized MNE, S_{cm} values using FO and SOC were on average approximately 9 mm, independent of the location of the sources and their spatial extent. In auditory cortex, using LOC resulted in S_{cm} = 8.1 mm, 8.1 mm, and 8.4 mm for dipoles, 10-mm, and 20-mm diameter cortical patches, respectively. In somatosensory cortex with LOC, S_{cm} = 8.7 mm, 8.5 mm, and 8.8 mm for dipoles, 10-mm, and 20-mm diameter extended sources, respectively, contrasted to 9.5 mm, 9.4 mm, and 10.0 mm, respectively, with FO, and 8.5 mm, 8.0 mm, and 8.0 mm, respectively, using SOC. Our simulations at somatosensory area indicated that using SOC could achieve the minimal S_{cm} compared to that using FO or LOC. Nevertheless, this benefit is less than 1 mm on average compared to the loose cortical orientation constraint inverse. Finally, MCE with LOC in auditory cortex gives the lowest averaged S_{cm} (7.8 mm for dipoles, 7.8 mm for 10-mm diameter sources, and 9.2 for 20-mm diameter sources). Using FO and SOC in MCE results in average shifts of 12 mm and 14 mm in auditory area. In the somatosensory area, MCE with dipole orientations taken from the free-orientation MNE resulted in average S_{cm} values of 2.9 mm, 4.0 mm, and 5.0 mm with dipoles, 10-mm diameter, and 20-mm diameter extended sources, respectively. If the dipole orientations are taken from MNE with LOC, the S_{cm} was reduced to 2.6 mm, 3.2 mm, and 3.6 mm with

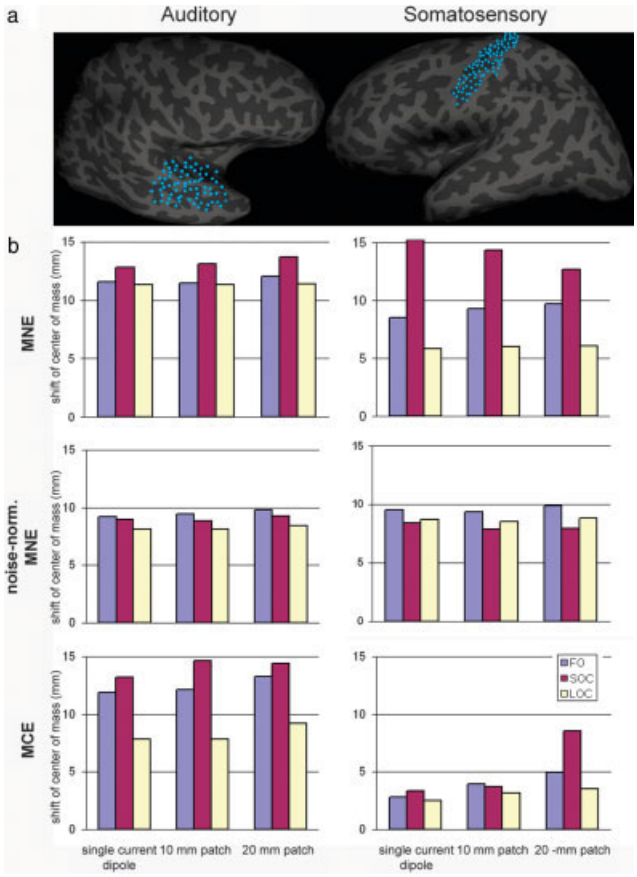

Figure 8.
The locations of the simulated current sources at the auditory cortex in the right hemisphere and the somatosensory cortex in the left hemisphere. Each blue dot represents an individually active current source. Three source extents were used: single dipole, 10-mm diameter patches, and 20-mm diameter patches (**a**). The average shift of center of mass from the center of the corresponding simulated source using minimum-norm estimates (MNE), noise-normalized MNE, and minimum-current estimate (MCE) in auditory and somatosensory areas (**b**). [Color figure can be viewed in the online issue, which is available at www.interscience.wiley.com.]

dipoles, 10-mm diameter, and 20-mm diameter simulated sources, respectively. MCE using a preliminary MNE with SOC gave averaged S_{cm} values of 3.4 mm, 3.7 mm, and 8.6 mm with single ECD, 10-mm diameter, and 20-mm diameter simulated sources, respectively.

Figure 9 shows the simulation results of MNE, noise-normalized MNE, and MCE when two sources are with 21-mm separation and are simultaneously active. In MNE, we found that using LOC with $\theta_d = 2.0\sigma_\theta$ can reduce the spatial distribution of the source estimates at the same threshold, as compared to using the free-orientation case. In addition, two loci of simulated sources were indicated by separate dorsal and ventral MNEs. In the noise-normalized MNE, LOC and FO can both provide estimates around two active loci. The noise-normalized MNE with SOC failed to produce two separate source estimates at the threshold to show the most significant 50% estimates. MCE with FO and SOC produces estimates with incorrect peak locations, either between the two synthetic sources or at the postcentral sulcus. Using LOC with $\theta_d = 2.0\sigma_\theta$, MCE can resolve two simultaneously active sources and localize them within 3-mm accuracy in the central sulcus.

Application to Auditory and Somatosensory MEG Data

We also employed data from auditory and somatosensory MEG experiments to test our methods in realistic situations. The experiments were conducted with healthy subjects un-

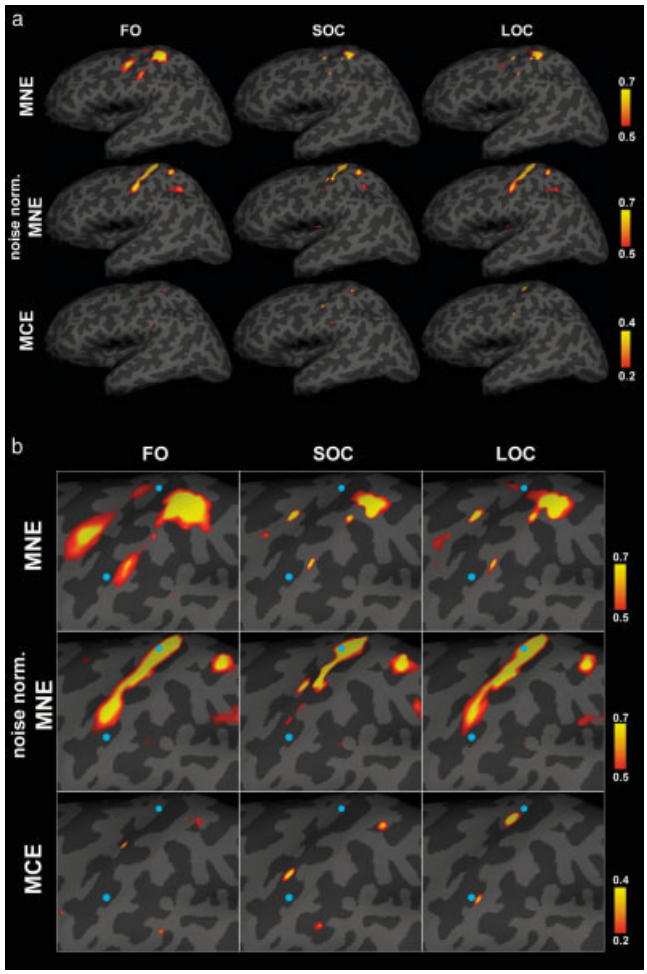

Figure 9.
Simulation with two simultaneously active dipole sources. The associated minimum-norm estimates (MNE), noise-normalized MNE, and minimum-current estimate (MCE) distributions are shown with dipole locations indicated with blue dots. Cortical current estimates were normalized between 0 and 1 to illustrate the spatial distributions.

der the approval of the institutional review board (IRB). Informed consent was obtained from the subjects before the experiments were carried out. In the auditory experiment, the stimuli were 60-ms wide-band noise bursts (2-kHz center frequency with 4-kHz bandwidth; 70-ms duration) presented binaurally. A 306-channel MEG system (Elekta-Neuromag, Ltd.) was used to record the neuromagnetic responses. The measurement bandwidth was 0.1–172 Hz and the data were digitized at 600 Hz. About 200 responses were averaged. In the somatosensory study, the right median nerve was stimulated at the wrist with 0.5-ms constant-current pulses whose amplitude was above the motor threshold. The interstimulus interval between the stimuli was 4 s. The measurement bandwidth was 0.03–250 Hz and the data were digitized at 1,004 Hz. About 100 responses were averaged.

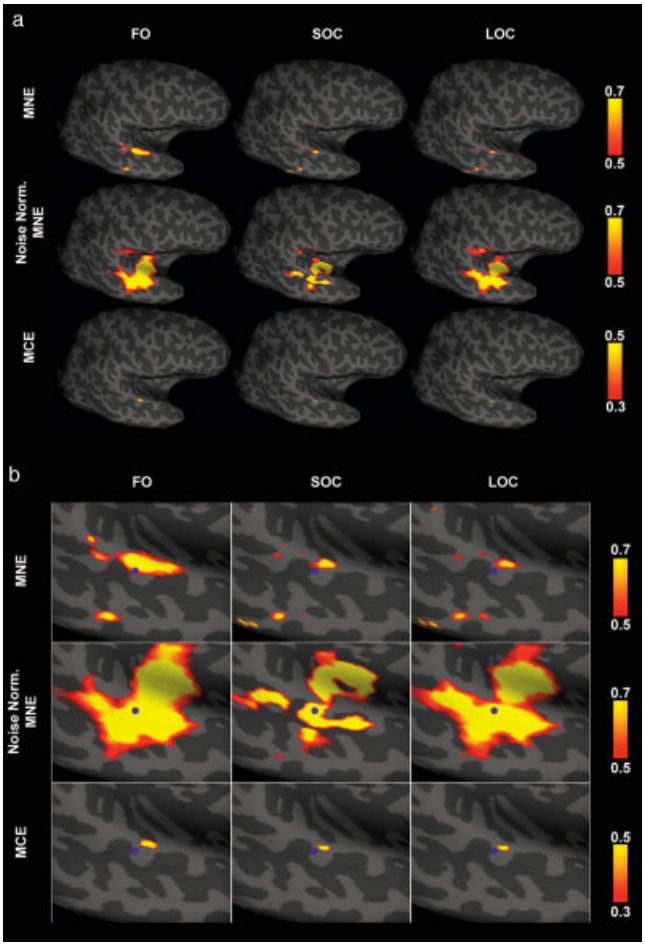

Figure 10.
Minimum-norm estimates (MNE), noise-normalized MNE, and minimum-current estimate (MCE) distributions at 98 ms after the onset of the auditory stimuli. The blue spot indicates the location of the corresponding equivalent current dipole (ECD). Cortical current estimates were normalized between 0 and 1 to illustrate the spatial distributions.

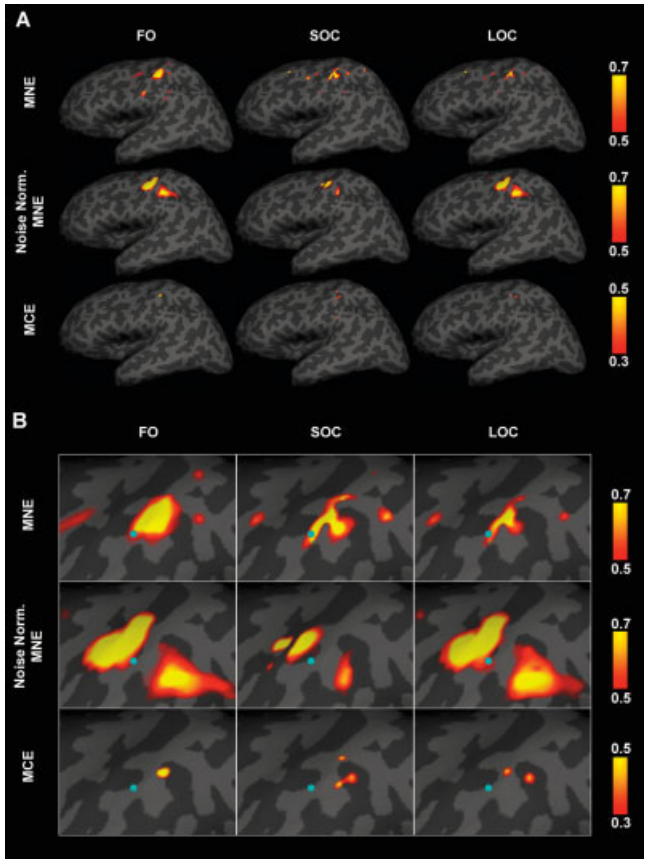

Figure 11.
Minimum-norm estimates (MNE), noise-normalized MNE, and minimum-current estimate (MCE) distributions at 50 ms after the onset of the median nerve stimulus. The blue spot indicates the location of the equivalent current dipole (ECD). Cortical current estimates were normalized between 0 and 1 to illustrate the spatial distributions.

To compare the results with discrete dipole modeling, we used the Xfit program (Elekta-Neuromag, Ltd.) to localize one ECD for both the auditory and somatosensory evoked-field experiments in each hemisphere. The location of the estimated single equivalent dipole was then displayed at the nearest location on the inflated white-matter surface.

For the auditory experiment, Figure 10 shows the MNE, noise-normalized MNE, and MCE of MEG recordings at 98 ms after the onset of the stimulus. The blue spot indicates the location of single equivalent dipole fitting, which is localized to the superior temporal gyrus (STG). Compared to MCE, MNE and noise-normalized MNE are more diffused. Both MNE and noise-normalized MNE resulted in fictitious sources around the medial temporal gyrus (MTG), in addition to the activity in STG. The distance between the ECD and the center of mass of MNE with FO, SOC, and LOC are reported in Table II. Figure 11 shows MNE and MCE of the somatosensory MEG experiment at 50 ms after the onset of stimulation. The ECD was located correctly at the postcen-

TABLE II. Shifts of the center of mass (S_{cm}) and maximum of the estimate (S_{max}) in millimeters from the equivalent current dipoles in the auditory experiment 50 ms after the onset of auditory stimulation

	FO		SOC		LOC	
Approach	S_{cm}	S_{max}	S_{cm}	S_{max}	S_{cm}	S_{max}
MNE	3.1	6.2	4.0	7.0	3.2	7.0
Noise-normalized MNE	11.0	15.0	10.9	12.5	11.6	15.0
MCE	7.8	7.8	2.2	7.5	6.5	7.0

FO, free orientation; SOC, strict orientation constraint; LOC, loose orientation constraint; MNE, minimum-norm estimate; MCE, minimum-current estimate.

tral gyrus. In MNE, it was found that the estimated activities were mostly from postcentral gyrus with minor activation in precentral gyrus. The distances between the center of mass of MNE and ECD with FO, SOC, and LOC are summarized in Table III. We found that using FO may generate the minimal or maximal shifts depending on whether we are measuring the center of mass or the maximum of the inverse solution. Both MNE and MCE using LOC gave consistently smaller shifts, regardless of whether it was being assessed by shift in the center of mass or shift in the maximum.

DISCUSSION

Structural MRI can provide precise information about the cortical geometry, including local cortical curvatures and the size of localized cortical patches. We employed the sizes of the patches to yield an estimate of the surface current density and the statistics of the cortical normals to compute distributed MEG source estimates where the current directions are loosely constrained by the cortical normals.

The incorporation of the LOC with $\theta_d = 2\sigma_\theta$–$3\sigma_\theta$ increases the accuracy of the localization, as shown in our simulation results in both auditory and somatosensory areas with dipolar or extended synthetic sources. In our simulations, we found that there is no unique optimal number across the whole brain for the best utilization of loose cortical orientation constraint in MNE and MCE. Presumably, this is due to the variations of cortical source space sampling and local anatomical curvature variations. However, in MNE, noise-normalized MNE, and MCE, we found that the utilization of LOC results in higher accuracy in localization and better resolution for simultaneously active sources. Our approach to employing LOC is different from the traditional implementation of MCE using MNE with unconstrained orientation to provide dipole orientation estimates [Uutela et al., 1999] and the MNE with a strict cortical orientation constraint [Liu et al., 1998]. The motivation of using a loose cortical orientation constraint is to retain a more accurate description of the cortical geometry when using a relatively sparse decimated source space. If the complete dense forward matrix could be employed in source estimation algorithms, such a loose cortical constraint may become unnecessary. In such a case, the price is the higher computational load in both ℓ^2-norm and especially ℓ^1-norm prior source modeling. In addition, the ill-posed nature of the MEG/EEG inverse with diffused point-spread and cross-talk metrics does not encourage the utilization of full gain matrix down to millimeter resolution [Liu et al., 2002]. The loose cortical constraint is thus a compromise for both computational efficiency and sufficient anatomical features in MEG/EEG inverse.

We employed the shift of center of mass to evaluate the accuracy of spatial localization and used dipole-fitting results as a gold standard for the location of the activation. Using single ECD fitting and mapping the result on the cortex may introduce some errors, because our ECD modeling does not restrict the solution on the cortex. The reasons for choosing the ECD as a gold standard are as follows. First, previous studies indicate that the realistic experimental data we employed (somatosensory median nerve stimulation and auditory stimulus) are generated by focal sources. Second, some simulations were based on single ECD-like point sources; thus the ECD is the correct true source in these cases. Third, using an ECD to

TABLE III. Shifts of the center of mass (S_{cm}) and maximum of the estimate (S_{max}) in millimeters from the equivalent current dipoles in the somatosensory experiment at 98 ms after onset of the median nerve stimulation

	FO		SOC		LOC	
Approach	S_{cm}	S_{max}	S_{cm}	S_{max}	S_{cm}	S_{max}
MNE	5.0	13.5	11.4	6.9	11.7	6.9
Noise-normalized MNE	9.5	11.2	8.7	7.5	8.7	13.5
MCE	6.9	6.9	5.7	5.7	5.7	5.7

FO, free orientation; SOC, strict orientation constraint; LOC, loose orientation constraint; MNE, minimum-norm estimate; MCE, minimum-current estimate.

model the MEG source is different from the distributed source modeling, such as MNE or MCE; thus, comparison based on ECD can avoid some common confounds in the distributed source modeling techniques. The reason to choose center of the mass of MNE/MCE inverse is to assess the localization results in a consistent and stable way. Previously, we used a similar strategy to assess the impact of functional MRI (fMRI) priors on the MNE [Liu et al., 1998]. In distributed source modeling, the spatial distribution is subjectively thresholded to illustrate the spatial distribution of current strength (in MNE and MCE) or the spatial distribution of statistical significance of brain activation (in noise-normalized MNE). There is no direct relationship between the center of mass in the distributed source modeling techniques and ECD fitting.

The other benefit of loose cortical orientation constraint in MNE is that it generates a less diffuse source estimate. This is because LOC allows a small source component tangential to the cortical surface to account for the MEG/EEG measurement. Although not as focal as MCE, MNE with LOC can potentially help the interpretation of localization results by reducing false spread of the source estimates to adjacent gyri or sulci, which in our experience were typical findings when applying a strict cortical orientation constraint.

We applied the proposed cortical constraints only on MEG data. Due to the similarity of the formulation of the source localization and physiological nature for signal genesis, such cortical constraints are expected to provide similar benefits in EEG localization in distributed source modeling.

In our approach, the source space has been generated by decimating the dense triangulation of the cortical surface without taking into account the spacing of undecimated vertices or the local curvature variations on the cortex. Using the patch statistics, it is in principle possible to refine the decimation in areas of high curvature, thus decreasing the variation of cortical normals within the patches. However, even with this eventual improvement in the selection of source locations, the LOC remains useful to alleviate problems arising from misalignment of the MEG and MRI coordinate frames when cortex normal information is employed in source analysis.

In conclusion, the LOC restricts the orientations of the sources to be approximately aligned with the cortical surface normal in each cortical source space location. This new approach reduces the problems apparent with a strict orientation constraint, which are due partly to the variation of the cortical normal direction within each cortical patch represented by the corresponding source space point and partly caused by misalignment of the MEG and MRI coordinate frames. We have demonstrated the utility of this novel approach in the computation of both ℓ^2 and ℓ^1 minimum-norm current estimates.

ACKNOWLEDGMENTS

We appreciate the comments from Drs. S.P. Ahlfors and N. Ille on the manuscript.

REFERENCES

Bertsekas DP (2000): Dynamic programming and optimal control. Belmont, MA: Athena Scientific.

Cohen D (1968): Magnetoencephalography: evidence of magnetic fields produced by alpha-rhythm currents. Science 161:784–786.

Dale A, Sereno M (1993): Improved localization of cortical activity by combining EEG and MEG with MRI cortical surface reconstruction: a linear approach. J Cogn Neurosci 5:162–176.

Dale AM, Fischl B, Sereno MI (1999): Cortical surface-based analysis. I. Segmentation and surface reconstruction. Neuroimage 9:179–194.

Dale AM, Liu AK, Fischl BR, Buckner RL, Belliveau JW, Lewine JD, Halgren E (2000): Dynamic statistical parametric mapping: combining fMRI and MEG for high-resolution imaging of cortical activity. Neuron 26:55–67.

Fischl B, Liu A, Dale AM (2001): Automated manifold surgery: constructing geometrically accurate and topologically correct models of the human cerebral cortex. IEEE Trans Med Imaging 20:70–80.

Fischl B, Sereno MI, Dale AM (1999): Cortical surface-based analysis. II: Inflation, flattening, and a surface-based coordinate system. Neuroimage 9:195–207.

Fuchs M, Wagner M, Kohler T, Wischmann HA (1999): Linear and nonlinear current density reconstructions. J Clin Neurophysiol 16:267–295.

Hämäläinen M, Hari R, Ilmoniemi R, Knuutila J, Lounasmaa O (1993): Magnetoencephalography—theory, instrumentation, and application to noninvasive studies of the working human brain. Rev Mod Phys 65:413–497.

Hämäläinen M, Ilmoniemi R (1984): Interpreting measured magnetic fields of the brain: estimates of current distributions. Helsinki, Finland: Helsinki University of Technology.

Hämäläinen MS, Sarvas J (1989): Realistic conductivity geometry model of the human head for interpretation of neuromagnetic data. IEEE Trans Biomed Eng 36:165–171.

Lin FH, Witzel T, Ahlfors SP, Stufflebeam SM, Belliveau JW, Hämäläinen MS (2004): Assessment and improvement on the spatial accuracy in MEG source localization by depth weighting corrected minimum-norm estimate. In: Bookheimer SY, Poline JB, Gulyas B, editors. Proceedings from the 10th annual meeting of the Organization for Human Brain Mapping. Budapest, Hungary. Elsevier Inc. p s46.

Liu AK, Belliveau JW, Dale AM (1998): Spatiotemporal imaging of human brain activity using functional MRI constrained magnetoencephalography data: Monte Carlo simulations. Proc Natl Acad Sci USA 95:8945–8950.

Liu AK, Dale AM, Belliveau JW (2002): Monte Carlo simulation studies of EEG and MEG localization accuracy. Hum Brain Mapp 16:47–62.

Matsuura K, Okabe Y (1995): Selective minimum-norm solution of the biomagnetic inverse problem. IEEE Trans Biomed Eng 42: 608–615.

Moon TK, Stirling WC (2000): Mathematical methods and algorithms for signal processing. Upper Saddle River, NJ: Prentice Hall.

Okada YC, Wu J, Kyuhou S (1997): Genesis of MEG signals in a mammalian CNS structure. Electroencephalogr Clin Neurophysiol 103:474-485.

Oostendorp TF, van Oosterom A (1989): Source parameter estimation in inhomogeneous volume conductors of arbitrary shape. IEEE Trans Biomed Eng 36:382–391.

Uutela K, Hämäläinen M, Salmelin R (1998): Global optimization in the localization of neuromagnetic sources. IEEE Trans Biomed Eng 45:716–723.

Uutela K, Hämäläinen M, Somersalo E (1999): Visualization of magnetoencephalographic data using minimum current estimates. Neuroimage 10:173–180.